PAPER

Toroidal modeling of resistive wall mode stability and control in HL-2M tokamak

IOP Publishing | International Atomic Energy Agency Nuclear Fusion

Nucl. Fusion **59** (2019) 016017 (15pp) https://doi.org/10.1088/1741-4326/aaf02c

Toroidal modeling of resistive wall mode stability and control in HL-2M tokamak

Guoliang Xia[1,2,a], Yueqiang Liu[1,3,a], C.J. Ham[2], Shuo Wang[1], Li Li[4], G.Y. Zheng[1], J.X. Li[1], N. Zhang[1], X. Bai[1], G.Q. Dong[1] and The HL-2M Team[b]

[1] Southwestern Institute of Physics, PO Box 432, Chengdu 610041, China
[2] CCFE, Culham Science Centre, Abingdon, OX14 3DB, United Kingdom of Great Britain and Northern Ireland
[3] General Atomics, PO Box 85608, San Diego, CA 92186-5608, United States of America
[4] College of Science, Donghua University, Shanghai 201620, China

E-mail: Guoliang.Xia@ukaea.uk and liuy@fusion.gat.com

Received 22 August 2018, revised 21 October 2018
Accepted for publication 12 November 2018
Published 13 December 2018

Abstract

Effects of toroidal plasma flow, magnetic drift kinetic damping as well as feedback control, on the resistive wall mode instability in HL-2M tokamak are numerically investigated, using the linear stability codes MARS-F/K (Liu *et al* 2000 *Phys. Plasmas* **7** 3681, Liu *et al* 2008 *Phys. Plasmas* **15** 112503). It is found that the precession drift resonance damping due to trapped thermal particles ensures a robust passive stabilization of the $n = 1$ (n is the toroidal mode number) RWM in the 2 MA double-null advanced plasma scenario designed for HL-2M, provided that the toroidal flow speed is not too fast: $\Omega_0 \leqslant 0.006\Omega_A$. With two rows of magnetic control coils designed for HL-2M, the optimal poloidal location for the RWM stabilization is found to be $\theta_c = 20°$–$22°$. Toroidal modeling also shows that the plasma flow damping, drift kinetic damping and magnetic feedback can be arranged to synergistically stabilize the RWM in HL-2M, by tuning the feedback gain phase and/or including derivative actions in the control loop. The numerical results obtained by MARS-F/K are qualitatively well re-produced by an analytic single-pole model.

Keywords: resistive wall mode, drift kinetic effects, feedback control, plasma flow, HL-2M tokamak

(Some figures may appear in colour only in the online journal)

1. Introduction

The HL-2M [1] is a new tokamak device currently under construction at Southwestern Institute of Physics, China. The designed plasma major radius and minor radius are 1.78 m and 0.65 m, respectively. HL-2M will install an ITER-like double-vacuum vessel and will be able to operate in double- or single-null configurations. One of the key missions of the HL-2M program is to explore high-performance tokamak plasma operation regimes, in particular the high beta long pulse advanced tokamak scenario, which is also foreseen for ITER [2]. The major obstacle for successful realization of such a scenario is the resistive wall mode instability. A systematic computational investigation of this instability for HL-2M is the scope of the present work.

The resistive wall mode (RWM) study has received much attention during recent years, because an unstable low-n (n is the toroidal mode number) RWM can limit the operational space of advanced tokamaks, including that designed for ITER [2]. The RWM can be viewed as a residual instability from the external ideal kink (XK) mode [3], which in turn is a global magneto-hydrodynamic (MHD) instability driven by plasma current and/or pressure. For a pressure driven XK, the stability is controlled by the normalized plasma pressure $\beta_N = \beta\,(\%)\,a\,(m)\,B_0\,(T)/I_p\,(MA)$, where β is the ratio of the volume averaged plasma pressure to the magnetic pressure, I_p the total plasma current, a the plasma minor radius, and B_0 the

[a] Author to whom any correspondence should be addressed.
[b] See author list of Duan *et al* 2017 Overview of recent HL-2A experiments Nucl. Fusion **57** 102013

vacuum toroidal magnetic field. When β_N exceeds a critical value (the so-called Troyon no-wall limit [4]), the XK becomes unstable. A close-fitting perfectly conducting wall can stabilize the XK, resulting in increased β_N. However, by replacing the ideal wall by a resistive wall, the resulting RWM grows on a timescale characteristic of the field penetration time through the wall. An unstable RWM brings the β_N limit back to the no-wall Troyon limit. It is thus highly desirable to achieve the RWM stabilization, in order to increase the plasma β_N for long pulse or steady state advanced tokamak operations.

The fact that the RWM grows very slowly, i.e. has a small (complex) mode frequency in the laboratory frame, has profound implication on the mode stabilization, either via passive means or via active control. Passive stabilization relies on the plasma toroidal rotation and drift kinetic resonances. Within the MHD theory, the free energy-releasing channels, that help to damp the RWM instability, include the ion sound wave damping and the shear Alfven wave continuum damping [5–9], which occur at finite plasma rotation frequency. The critical rotation velocity, required for complete stabilization of the mode, is normally a few percent of the Alfven speed [5]. Inclusion of drift kinetic resonances, in particular that due to the toroidal precession of trapped thermal particles, has been shown to substantially enhance the mode stability at slow plasma flow [10–14]. The drift kinetic theory thus successfully explains the experimental observations in DIII-D [15] and JT-60U [16], where a plasma toroidal flow of about 0.3% of Alfven speed was found to completely stabilize the RWM.

Active control of the RWM, using magnetic coils [13, 17–22], is feasible thanks to the relatively slow growth of the instability. The basic idea of feedback stabilization of the RWM is to use the magnetic field, produced by current-carrying coils, to actively compensate the field perturbation produced by the mode instability. Feedback experiments carried out in both tokamaks [23, 24] and reversed field pinches [25, 26] have demonstrated successful active control of the RWM, up to the ideal wall beta limit.

In this paper, we focus on studying the $n = 1$ RWM stability and control for the HL-2M tokamak. As indicated above, a reasonably comprehensive investigation of the RWM behavior in a new device should consider the magnetic drift kinetic effects, the toroidal flow of the plasma, the active control using magnetic coils, as well as the possible synergy effect between passive and active means.

The multiple aspects of the problem force us to explore the mode stability in multi-dimensional space. The parameters that we vary in this study include: the plasma pressure, the radial distance of the double resistive wall, the plasma toroidal rotation speed, the poloidal location of the feedback coils, as well as the controller parameters (feedback gain amplitude and phase, the proportional versus derivative actions). We use the MARS-F [17] and MARS-K [27] codes for our computational study. The numerical results are qualitatively verified by an analytic model where possible.

The next section describes the computational models and introduces a reference equilibrium designed for HL-2M. Section 3 reports numerical and analytic results. Section 4 draws conclusions.

2. Computational models and HL-2M equilibrium

2.1. Computational models in MARS-F/K

Each of the physics models of the MARS-F/K codes (the single fluid mode with toroidal flow [5, 6], the MHD-kinetic hybrid formulation [27], magnetic feedback [28]), that are relevant to the RWM and that we shall employ in this study, has previously been reported in separate publications. For the completeness of discussions, we present below a brief overview of these models.

The core fluid equations in the plasma region, which are solved by MARS-F/K, are written in the Eulerian frame [27, 29]

$$(\gamma + in\Omega)\,\boldsymbol{\xi} = \mathbf{v} + (\boldsymbol{\xi}\cdot\nabla\Omega)\,R^2\nabla\phi \tag{1}$$

$$\rho\,(\gamma + in\Omega)\,\mathbf{v} = -\nabla\cdot\mathbf{p} + \mathbf{j}\times\mathbf{B} + \mathbf{J}\times\mathbf{b} - \rho\left[2\Omega\widehat{\mathbf{Z}}\times\mathbf{v} + (\mathbf{v}\cdot\nabla\Omega)\,R^2\nabla\phi\right] - \nabla\cdot\boldsymbol{\Pi} \tag{2}$$

$$(\gamma + in\Omega)\,\mathbf{b} = \nabla\times(\mathbf{v}\times\mathbf{B}) + (\mathbf{b}\cdot\nabla\Omega)\,R^2\nabla\phi \tag{3}$$

$$(\gamma + in\Omega)\,p = -\mathbf{v}\cdot\nabla P - \Gamma P\nabla\cdot\mathbf{v} \tag{4}$$

$$\mu_0\mathbf{j} = \nabla\times\mathbf{b} \tag{5}$$

where γ is the (generally complex) eigenvalue of the instability, corrected by a Doppler shift $in\Omega$. Ω is the angular frequency of the plasma flow along the toroidal angle ϕ. The lower-case quantities $(\boldsymbol{\xi}, \mathbf{v}, \mathbf{b}, \mathbf{j}, \mathbf{p})$ represent the plasma displacement, perturbed velocity, magnetic field, current and pressure tensor, respectively. The perturbed pressure tensor $\mathbf{p} = p\mathbf{I}$ in the fluid approximation, where p is a scalar quantity and $\mathbf{I}$ the unit tensor. The upper-case symbols are equilibrium quantities, obtained by the equilibrium code CHEASE [30]. ρ is the unperturbed mass density, R the plasma major radius, $\widehat{\mathbf{Z}}$ the unit vector in the vertical direction. $\boldsymbol{\Pi}$ is a viscous stress tensor, chosen in this work to represent a viscous force damping of the parallel sound wave [6], with a numerical coefficient $\kappa_\parallel$ specifying the strength of the damping.

The MHD-kinetic hybrid formulation (MARS-K) differs from the fluid formulation (MARS-F) in the closure for the second momentum. The perturbed pressure tensors $\mathbf{p}$, that enters into the momentum equation (2), consists of three parts in MARS-K [31, 32]

$$\mathbf{p} = p\mathbf{I} + p_\parallel\widehat{\mathbf{b}}\widehat{\mathbf{b}} + p_\perp\left(\mathbf{I} - \widehat{\mathbf{b}}\widehat{\mathbf{b}}\right) \tag{6}$$

where $\widehat{\mathbf{b}} = \mathbf{B}/B$, $B = |\mathbf{B}|$. The scalar quantity p is the isotropic contribution representing the so-called adiabatic part of the drift kinetic pressure. The anisotropic pressure perturbations $p_\parallel(\boldsymbol{\xi}_\perp)$ and $p_\perp(\boldsymbol{\xi}_\parallel)$, parallel and perpendicular to the equilibrium magnetic field lines, respectively, come from the non-adiabatic contributions. The non-adiabatic pressure tensor terms effectively replace the compressibility term $\Gamma P\nabla\cdot\mathbf{v}$ from the fluid closure, equation (4). For thermal particles with Maxwellian equilibrium distribution, the adiabatic contribution exactly recovers the convective term of equation (4)

[33]. In this study, we consider drift kinetic effects from thermal particles only. The perturbed kinetic pressure tensors are calculated via a semi-analytic solution of the linearized drift kinetic equation in the continuum form without geometrical simplifications (i.e. in full toroidal geometry) [31]. The key physics associated with the drift kinetic solution is described by the mode-particle resonance operator λ_{ml}

$$\lambda_{ml} = \frac{n\left[\omega_{*N} + \left(\hat{\varepsilon}_k - 3/2\right)\omega_{*T} + \omega_{\mathrm{E}}\right] - \omega}{n\omega_{\mathrm{d}} + \left[\alpha\left(m + nq\right) + l\right]\omega_{\mathrm{b}} - \omega} \tag{7}$$

where ω_{*N} and ω_{*T} are the diamagnetic drift frequencies due to the density and temperature gradients, respectively. ω_{E} is the $\mathbf{E}\times\mathbf{B}$ drift frequency due to the equilibrium electrostatic potential. $\hat{\varepsilon}_k = \varepsilon_k/T$ is the particle kinetic energy normalized by temperature T. $\omega_{\mathrm{d}} = \langle\dot{\phi}\rangle$ is the bounce-orbit-averaged toroidal precession drift frequency of particles, including the ω_{E} drift. ω is the mode (complex) frequency, with $\gamma = -\mathrm{i}\omega$. q is the safety factor. We have neglected the effect of finite radial excursion width of particles across the magnetic surfaces. The parameter $\alpha = 0$ for trapped particles, with ω_{b} denoting the bounce frequency; and $\alpha = 1$ for passing particles, with ω_{b} denoting the transit frequency. In this study, we shall consider the magnetic precession of trapped thermal ions and electrons, as well as the bounce motion of trapped thermal ions.

In order to model active control of the RWM, we assume a basic feedback law, where the magnetic signal $\psi_{\mathrm{s}}(t)$, measured by a set of sensor loops, is used to determine the current I_{f} flowing in the active coils [17]

$$M_{\mathrm{sf}}I_{\mathrm{f}} = -G\psi_{\mathrm{s}}(t) \tag{8}$$

where G is the (complex) feedback gain, $G = |G|\,\mathrm{e}^{\mathrm{i}\phi}\left(1 + \alpha_{\mathrm{D}}\gamma\tau_{\mathrm{F}}\right)$ for a PD controller. Here, $|G|$ and ϕ represent the amplitude and phase of the feedback gain, respectively. α_D measures the ratio of derivative to proportional gains, and τ_{F} is the L/R time of the active coils. Note that α_{D} can generally be a complex number. In this work, however, we vary α_{D} only along the real axis, in order to keep a reasonable dimension of parameter space. $\psi_{\mathrm{s}}(t)$ is assumed to be a pointwise poloidal field signal in this work. M_{sf} is the free-space mutual inductance between the feedback coil and the sensor loop, used largely to normalize the feedback gain.

We also define an open-loop transfer function $P(s)$

$$P(s) = \frac{\psi_{\mathrm{s}}}{M_{\mathrm{sf}}I_{\mathrm{f}}} \tag{9}$$

where s is the Laplace variable representing the mode eigenvalue. It is important to note that $P(s)$ can be computed as the plasma response to a given current source flowing in the active coils. Equations (8) and (9) are combined to yield the closed-loop characteristic equation

$$1 + GP(s) = 0. \tag{10}$$

The solution of the characteristic equation gives the closed loop eigenvalue s, for a chosen feedback gain G. This offers an alternative way of computing the closed loop eigenvalue, as compared to the direct solution of the MHD and feedback equations. We shall employ and cross-check both approaches in this study.

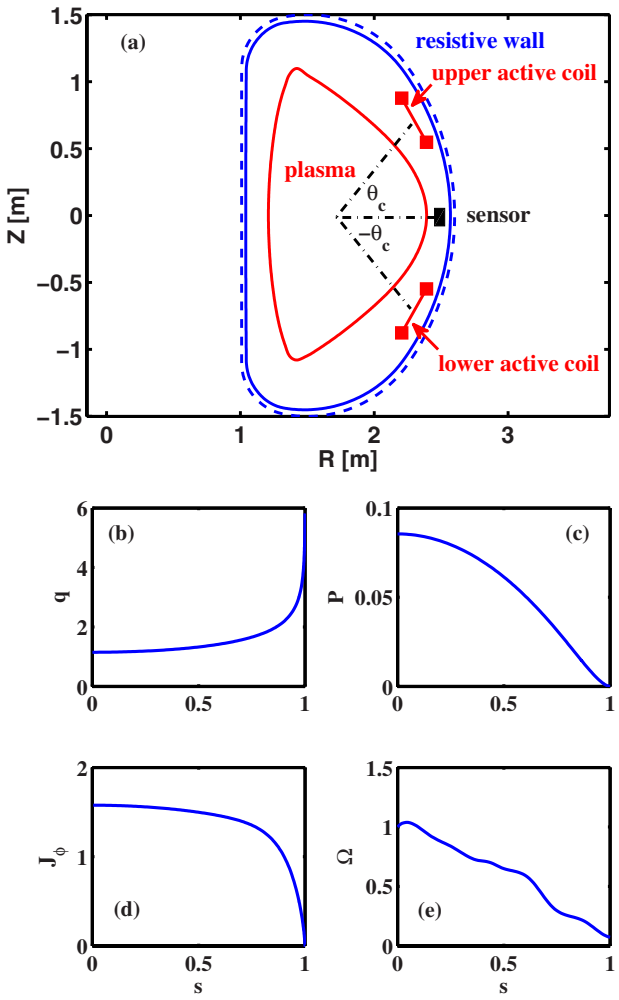

Figure 1. (*a*) Geometry of the HL-2M tokamak with the plasma in a double-null configuration and with a double-wall vacuum vessel. Sketched are also the locations of active and sensor coils for magnetic feedback. Shown also are equilibrium radial profiles for (*b*) the safety factor, (*c*) the plasma pressure normalized by B_0^2/μ_0, (*d*) the surface averaged toroidal current density normalized by $B_0/(\mu_0 R_0)$, and (*e*) the assumed plasma toroidal rotation frequency normalized by $\Omega_A = B_0/\left(R_0\sqrt{\mu_0\rho_0}\right)$. Here $s = \sqrt{\psi_{\mathrm{p}}}$ labels the plasma minor radius, with ψ_{p} being the normalized poloidal equilibrium magnetic flux.

2.2. HL-2M equilibrium and control coil geometry

We consider an equilibrium from the 2 MA high performance scenario designed for HL-2M equilibrium [34], with double-null plasma configuration. The plasma boundary shape is shown in figure 1(*a*). The key equilibrium radial profiles are plotted in figures 1(*b*)–(*e*). The on-axis safety factor is $q_0 = 1.14$. The safety factor at 95% of the magnetic flux surface is $q_{95} = 3.1$. We point out that no design prediction for the toroidal rotation is presently available for HL-2M. The rotation profile shown in figure 1(*d*) is numerically assumed. The amplitude of the rotation frequency will be scanned in our investigation.

The target plasma has the normalized beta value of $\beta_N = 4.74$. The MARS-F computed Troyon no-wall beta limit is $\beta_N^{\text{no-wall}} = 3.63$, and the ideal-wall beta limit is $\beta_N^{\text{ideal-wall}} = 5.65$. The ideal wall corresponds to the inner vacuum vessel shown in figure 1(*a*), with $d/a = 1.3$. This relatively large width of the β_N window (the distance between the no-wall and ideal-wall limits) for the RWM regime is mainly due to the broad current profile (figure 1(*d*)) designed for this target HL-2M scenario. A plasma with low internal inductance tends to be subject to more wall stabilization [35]. As usual, we define the pressure scaling factor $C_\beta = \left(\beta_N - \beta_N^{\text{no-wall}}\right)/\left(\beta_N^{\text{ideal-wall}} - \beta_N^{\text{no-wall}}\right)$ for the RWM study. This factor is 0.55 for the target plasma in HL-2M design. The effective wall time of the double vacuum vessel ($d/a = 1.3, 1.35$) in HL-2M is estimated to be $\tau_w = \mu_0 h_w L/(2\pi\eta_w) = 2.2 \times 10^4 \tau_A$. Here, τ_A is the toroidal Alfven time, h_w the wall thickness, L the poloidal length of the wall, and η_w the resistivity of the vacuum vessel.

Two rows of in-vessel magnetic coils are designed for HL-2M: the upper and lower rows, respectively (figure 1(*a*)), with each row consisting of eight window-frame coils along the toroidal angle. The poloidal coverage of each coil is $\Delta\theta = 21.8°$ (measured in the geometric angle with origin defined as the magnetic axis). These coils will also be used for passive control of type-I edge localized mode (ELM) in HL-2M. The poloidal angle of the center of each coil (to be referred to as the poloidal location), θ_c, is designed to be $\theta_c^U = -\theta_c^L = 29.9°$ (again in geometric angle). Finally, for active control, the sensor coils are located at the outboard mid-plane and just inside the vacuum vessel, measuring the poloidal component of the magnetic field perturbation.

3. Numerical versus analytic results

In what follows, we investigate several mechanisms for the RWM stabilization in HL-2M tokamak. These include: toroidal flow stabilization, drift kinetic damping due to plasma thermal particles, magnetic feedback stabilization. Each of the aforementioned physics can act alone or in combination with the others. For instance, plasma flow alone can stabilize the RWM via Alfven or sound wave continuum resonances [3], as well as ion Landau resonance induced parallel sound wave damping [36]. In combination with drift kinetic physics, plasma toroidal flow helps to create kinetic resonance conditions for the RWM [10, 27, 37]. Combining plasma flow and magnetic feedback helps to explore the synergistic effects between continuum wave damping, parallel sound wave damping, and active stabilization of the mode [38]. Finally, drift kinetic resonances coupled to magnetic feedback provides another synergy [39]. All these effects will be considered in this work, in order to obtain relatively comprehensive understanding of the $n = 1$ RWM stability in HL-2M.

3.1. Kinetic effects on the RWM stability in HL-2M

We start by investigating the effects of drift kinetic resonances on the RWM in HL-2M plasmas. No magnetic feedback is assumed here. We shall consider kinetic stabilization of the mode due to precessional and bounce resonances of trapped thermal particles. The transit resonance of passing particles normally provides too weak effect on the RWM in tokamak plasmas.

Note that we only pursue the so-called non-perturbative computations [27, 33] for the RWM in this study, due to the fact that the non-perturbative approach allows (i) kinetic modification of the eigenfunction of the (fluid) RWM, and (ii) more self-consistent treatment of the kinetic resonances (i.e. the RWM eigenvalue self-consistently enters into the kinetic resonance operator (7)), the mode computed by the non-perturbative approach is normally more unstable than that predicted by the perturbative approach [27, 33]. The non-perturbative approach thus provides a more conservative estimate of the RWM instability. In other words, if the mode is predicted to be stable (or feedback stabilized) by the non-perturbative approach, as in this work, the mode would mostly be even more stable according to the perturbative prediction.

In order to understand the transition of the mode stability from the fluid RWM to the kinetic RWM, we introduce a numerical factor α denoting the kinetic fraction to be included into the MARS-K MHD-kinetic hybrid computations. Hence $\alpha = 0$ recovers the fluid limit, whilst $\alpha = 1$ corresponds to the physically relevant full inclusion of the corresponding kinetic resonance effect.

Figure 2(*a*) shows two representative examples of the MARS-K computed mode eigenvalue, while scanning the kinetic fraction factor $\alpha_P\,(= \alpha)$ from 0 to 1, for the precessional drift resonance contribution from trapped thermal ions and electrons. The target plasma of the HL-2M advanced scenario design is assumed here ($C_\beta = 0.55$). Two choices of the plasma toroidal rotation frequency are considered, with the on-axis values of $\Omega_0 = 0.006\Omega_A$ (representing slow flow) and $\Omega_0 = 0.01\Omega_A$ (representing fast flow), respectively. Note that in these computations, the parallel sound wave damping coefficient is kept very small $\kappa_{||} = 0.1$. Most of the damping comes from the drift kinetic resonances. In particular, figure 2(*a*) shows that the precessional drift resonance provides more stabilization at slower plasma flow. At 0.6% of Alfven speed for the on-axis toroidal flow, the $n = 1$ RWM in HL-2M design target plasma can be fully stabilized already with about 60% fraction of the precessional drift kinetic damping from trapped thermal ions and electrons. In other words, the mode should be passively stabilized by the precessional drift resonances at slow flow.

A faster flow (e.g. at 1% of Alfven speed as shown in figure 2(*a*)) does not result in full stabilization of the mode, but nevertheless yielding more than one order of magnitude reduction of the mode growth rate. At a faster flow, it is often expected that the bounce resonance of trapped thermal ions can provide certain stabilization to the RWM. This additional stabilization is found to be very weak for this HL-2M plasma, as shown by figure 2(*b*).

Figure 3 further demonstrates that most of the damping comes from the precessional drift resonances ($\alpha_P = 1$). Without these resonances ($\alpha_P = 0$), i.e. with only the fluid continuum resonances and a weak ($\kappa_{||} = 0.1$) parallel sound

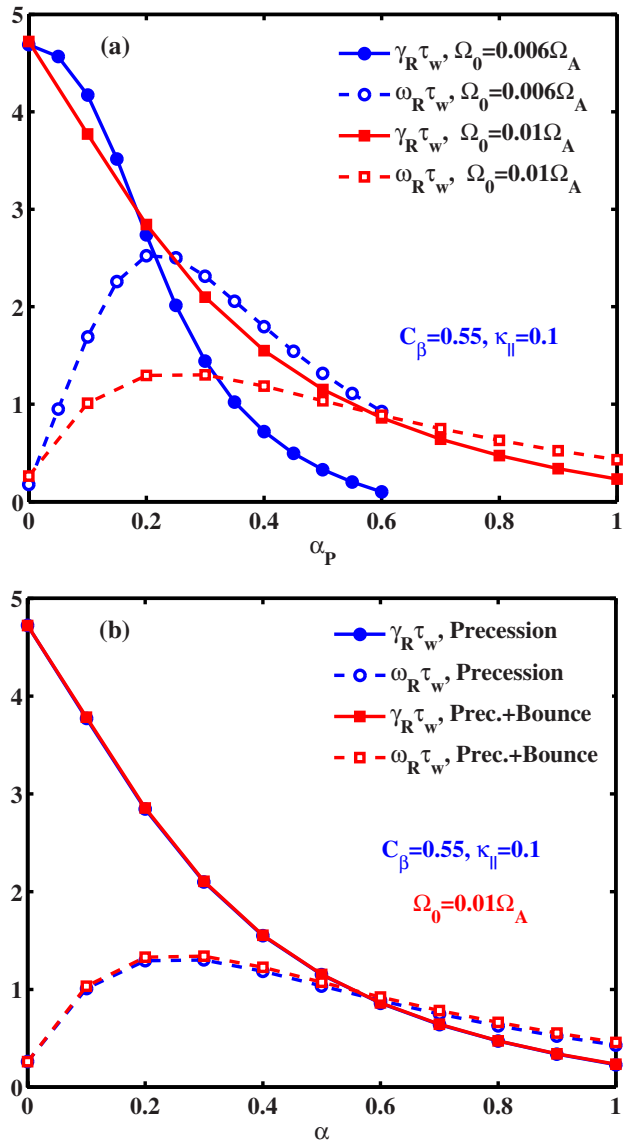

Figure 2. Growth rate (solid lines) and mode frequency (dashed lines) of the MARS-K computed $n = 1$ RWM versus the kinetic fraction factor for (a) precessional drift resonance alone at two choices of the plasma toroidal rotation frequencies, $\Omega_0 = 0.006\Omega_A$ (circles) and $\Omega_0 = 0.01\Omega_A$ (squares), (b) two choices of kinetic resonances—precession alone and precession combined with bounce resonance of trapped thermal ions, at fixed plasma rotation $\Omega_0 = 0.01\Omega_A$. Note that the curves with these two choices of kinetic resonances nearly overlap with each other. The other parameters are fixed: the normalized wall distance $d/a = 1.3, 1.35$, the plasma pressure $C_\beta = 0.55$ and the parallel viscous damping coefficient $\kappa_\| = 0.1$.

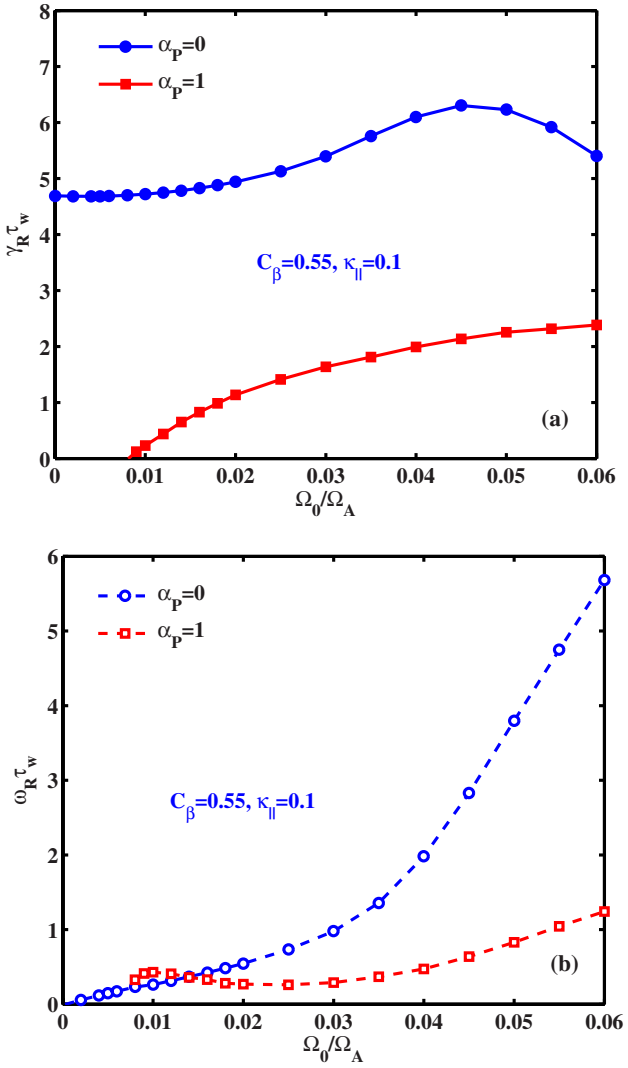

Figure 3. (a) Growth rate and (b) mode frequency of MARS-K computed $n = 1$ RWM versus the plasma on-axis rotation frequency, for two choices of physics models—the fluid model ($\alpha_P = 0$) versus the drift kinetic model ($\alpha_P = 1$) with precessional drift resonaces of trapped thermal particles. The other parameters are fixed: the normalized wall distance $d/a = 1.3, 1.35$, the plasma pressure $C_\beta = 0.55$, and the parallel viscous coefficient $\kappa_\| = 0.1$.

wave damping, the mode stability is hardly modified by the plasma flow. In fact, a slight destabilization occurs at $\Omega_0 \sim 0.04\Omega_A$ via Kelvin–Helmholtz mechanism associated with flow shear. The precessional drift kinetic stabilization opens a stability window for the RWM, at slow toroidal flow $\Omega_0/\Omega_A = (0, 0.008)$, for this HL-2M plasma.

According to the drift kinetic model, full suppression of the RWM is possible even vanishing flow as shown in figure 3, thanks to the so-called precessional drift reversal effect, where the toroidal precession of banana orbit of trapped particles changes direction depending on the particle pitch angle. This effect, shown to be caused by the plasma diamagnetism [40], means that the kinetic resonance can occur even at vanishing plasma flow, at certain particle pitch angle. This can generate sufficient damping to fully suppress the RWM. On the other hand, no full stabilization has been observed in experiments at vanishing flow [15, 16]. There can be different reasons. One plausible explanation is the existence of a small but finite residual error field (after the best correction in experiments), which can still destabilize the mode.

One of the major goals of HL-2M tokamak is to achieve high pressure, high density, long pulse or steady state plasmas. It is therefore of a critical issue to access stable domain for the RWM and at the same time maintaining high plasma pressure. Because the plasma flow speed and the precessional drift resonance damping are the two key factors in the RWM stabilization (figure 3), we again consider this kinetic resonance

effect ($\alpha_P = 1$) and map out the stable domain in the 2D space defined by the plasma flow speed and the equilibrium pressure scaling factor. Such a stable domain, plotted in figure 4(*a*), provides quantitative guidance for the high-beta plasma discharge operations in HL-2M. In particular, we note that a robustly stable domain (against plasma pressure variation) can be accessed, if the toroidal plasma rotation is sufficiently slow: $\Omega_0 \leqslant 0.006\Omega_A$.

3.2. Feedback stabilization of the RWM in HL-2M

An alternative approach for stabilizing the RWM is to use magnetic coils for active control. As mentioned before, the present 3D field coil designed in HL-2M assumes two rows of active coils located at the upper and lower half-plane of the low field side of the torus, and just inside the vacuum vessel. We refer to them as the upper and lower rows of coils in this work. These coils, whose exact geometrical poloidal location has not yet been fully decided, are also planned to be used for controlling edge localized modes in HL-2M.

As for the sensor coils for the RWM feedback stabilization, we shall assume a single row of pick-up coils located at the outboard mid-plane and just inside the inner vacuum vessel (figure 1(*a*)), measuring the poloidal component of the perturbed $n = 1$ magnetic field. This is conventionally referred to as the internal poloidal sensors, which provide superior performance over the radial sensors [17], for the RWM control. In the closed loop system, this single row of sensor single is connected to drive the coil currents in the two rows of active coils, via two separate controllers represented by the upper and lower row feedback gains in this work. This is often referred to as multiple-input-single-output (MISO) control.

In this subsection, we shall only consider the fluid model (MARS-F). We include the strong parallel sound wave damping model [38], with a numerical damping coefficient of $\kappa_{\|} = 1.5$, in order to mimic the thermal ion Landau damping physics [41]. In the following subsection 3.3, we shall consider cases where the parallel sound wave damping model is replaced by the more accurate drift kinetic damping models in MARS-K.

Figure 5(*a*) shows the first set of results, where we scan the feedback gain amplitude for both the upper and lower rows of active coils, and compute the closed loop eigenvalue for the HL-2M design target plasma. With a naïve choice of the gain phase, $\phi_U = 0°, \phi_L = 0°$, the proportional feedback control destabilizes the RWM for $\theta_c = 29.9°$ (the designed poloidal location), however, the mode can be stabilized for $\theta_c = 20.7°$ (an optimal poloidal location shall be reported in a later figure) with large gain amplitude. Moreover, feedback stabilization of the mode with $\theta_c = 29.9°$ can be achieved with a better choice of the gain phase, e.g. $\phi_U = 60°, \phi_L = -30°$ as shown in figure 5(*b*). In fact, this gain phase, which is not yet the best choice (gain phase optimization shall be reported in a later figure), leads to the mode stabilization also for varying plasma pressures. For the design target plasma ($C_\beta = 0.55$), the $n = 1$ RWM is stabilized at a critical gain value of $|G| = 2.1$. The

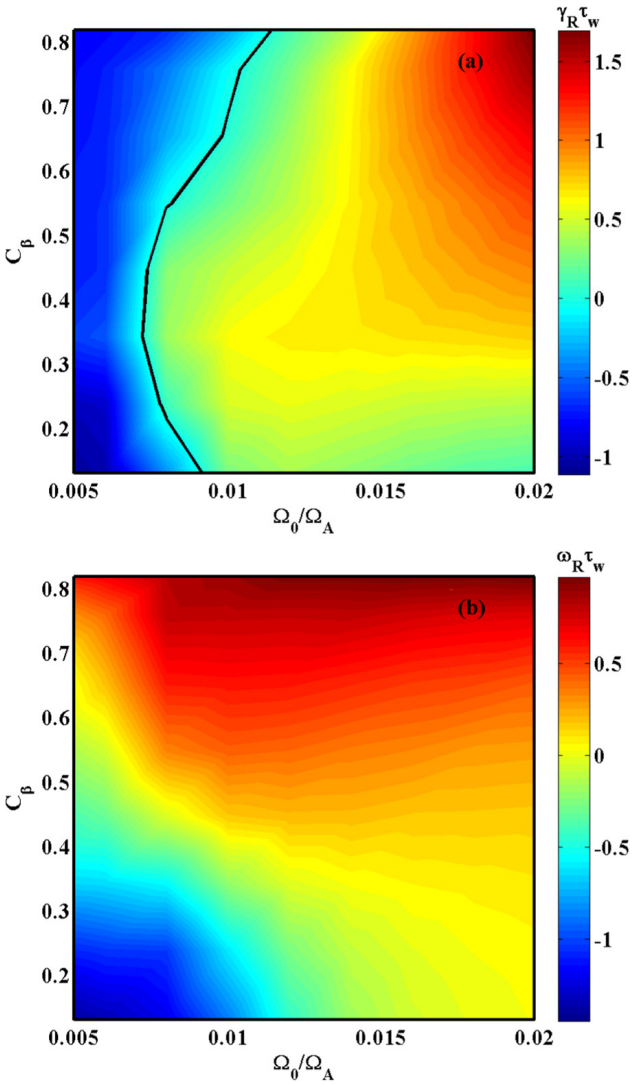

Figure 4. Contour plots of (*a*) growth rate and (*b*) mode frequency of the MARS-K computed $n = 1$ kinetic RWM in the 2D parameter space $C_\beta - \Omega_0/\Omega_A$, with inclusion of the precessional drift resonances of trapped thermal particles ($\alpha_P = 1$). The other parameters are fixed at $d/a = 1.3, 1.35$ and $\kappa_{\|} = 0.1$. The solid curve in (*a*) indicates the stability boundary in the 2D domain.

critical gain value increases with increasing the equilibrium pressure, as expected.

An important control design issue for HL-2M is the poloidal location of the active coils. Figure 6 plots the MARS-F computed critical proportional gain required for the $n = 1$ RWM stabilization, on the poloidal location angle θ_c. It is evident that there is an optimal poloidal location of the active coil, at $\theta_c = 20°$–$22°$, that minimizes the feedback efforts. Moreover, this optimal location does not seem to be sensitive to the variation of the plasma pressure (figure 6(*a*)), nor to the feedback gain phase (within certain ranges) (figure 6(*b*)).

The coil location is presently preliminary designed at $\theta_c = 29.9°$ in HL-2M, following geometrical constraint on the device. This is not the optimal choice according to the MARS-F simulations. Figure 7 compares the Nyquist plots of the open loop transfer functions $P(j\omega)$, computed for $\theta_c = 29.9°$

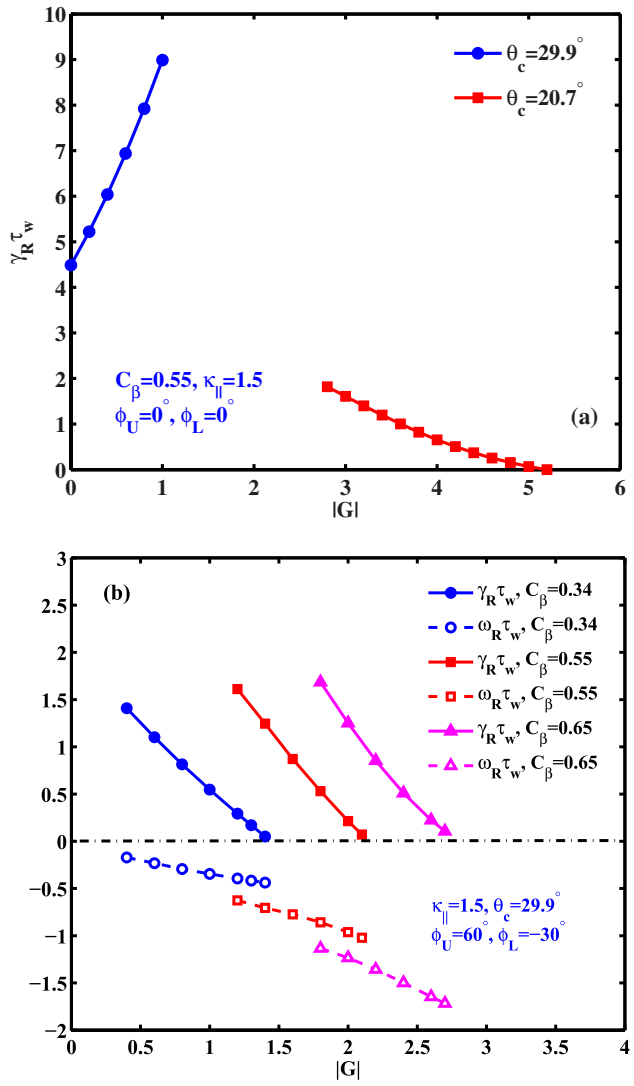

Figure 5. (*a*) The MARS-F computed growth rate of the $n = 1$ RWM versus the proportional feedback gain amplitude, at fixed gain phase $\phi_U = 0°, \phi_L = 0°$ associated with the upper and lower rows of active coils, and for two poloidal locations of active coils, $\theta_c = 29.9°$ (circles) and $\theta_c = 20.7°$ (squares), respectively. The mode frequency vanishes (not shown). (*b*) The growth rate (solid lines) and mode frequency (dashed lines) of the RWM versus the proportional feedback gain amplitude at fixed gain phase $\phi_U = 60°, \phi_L = -30°$, for three choices of the plasma equilibrium pressure: $C_\beta = 0.34$ (circles), $C_\beta = 0.55$ (squares) and $C_\beta = 0.65$ (triangles), respectively. The other parameters are fixed: the normalized wall distance $d/a = 1.3, 1.35$, the radial and poloidal locations of the active coils $r_f/a = 1.29$ and $\theta_c = 29.9°$, the poloidal coverage of the coils $\Delta\theta = 21.8°$, the radial location of the sensors $r_s/a = 1.29$, and the parallel viscous coefficient $\kappa_{||} = 1.5$. No plasma rotation is assumed in these computations.

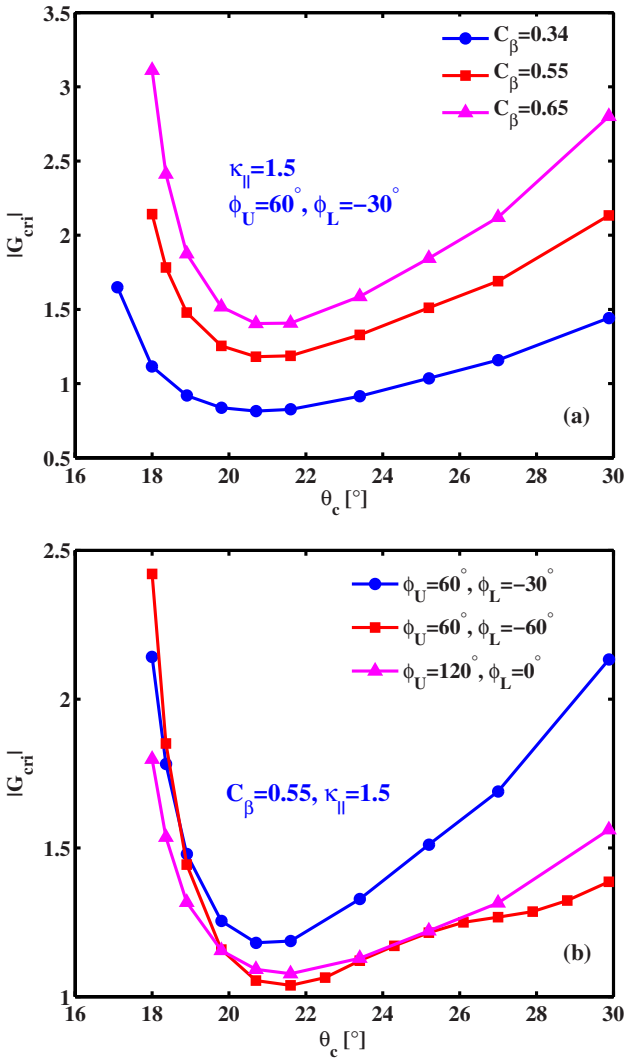

Figure 6. The MARS-F computed minimal proportional feedback gain amplitude for full stabilization of the $n = 1$ RWM, versus the poloidal location of active coils for (*a*) different plasma pressures $C_\beta = 0.34$ (circles), $C_\beta = 0.55$ (squares) and $C_\beta = 0.65$ (triangles) at fixed gain phase $\phi_U = 60°, \phi_L = -30°$, and (*b*) different gain phases $\phi_U = 60°, \phi_L = -30°$ (circles), $\phi_U = 60°, \phi_L = -60°$ (squares) and $\phi_U = 120°, \phi_L = 0°$ (triangles) at fixed pressure $C_\beta = 0.55$. The other parameters are fixed at $d/a = 1.3, 1.35$, $r_f/a = 1.29$, $r_s/a = 1.29$, $\Omega_0 = 0$ and $\kappa_{||} = 1.5$.

and $\theta_c = 20.7°$ (the optimal location according to figure 6), respectively, and plotted in the complex plane. According to the Cauchy principle of phase variation, the closed loop stabilizes the unstable mode, if and only if the corresponding Nyquist contour $GP(j\omega)$ counter-clockwise encircles $(-1, 0)$ in the complex plane, as the frequency ω increases from $-\infty$ to $+\infty$. The Nyquist plots shown in figure 7 thus indicate that, with the gain phase of $\phi_U = 0°, \phi_L = 0°$ and with the poloidal location of the active coils at $\theta_c = 20.7°$, the RWM can be fully stabilized at sufficiently large proportional gain ($|G| \geqslant 5.2$, as shown in figure 5(*a*)). The mode cannot be feedback stabilized even with infinite gain amplitude, with the designed coil location of $\theta_c = 29.9°$ for HL-2M and with zero gain phase. This also corroborates the direct feedback computation results shown in figure 5(*a*).

On the other hand, the Nyquist curve shown in figure 7, for the case of $\theta_c = 29.9°$, indicates that feedback with gain phase $\phi_U = \phi_L = \arg(G) = -180°$ can stabilize the RWM. This is indeed the case as shown in figure 8. In fact, a range of gain phase can be chosen, where the mode can be fully stabilized with a finite critical gain amplitude. Moreover, figure 8 shows that two approaches predict nearly the same critical gain values. One approach (solid line) is based on the MARS-F computed open loop transfer functions (with Nyquist analysis similar to

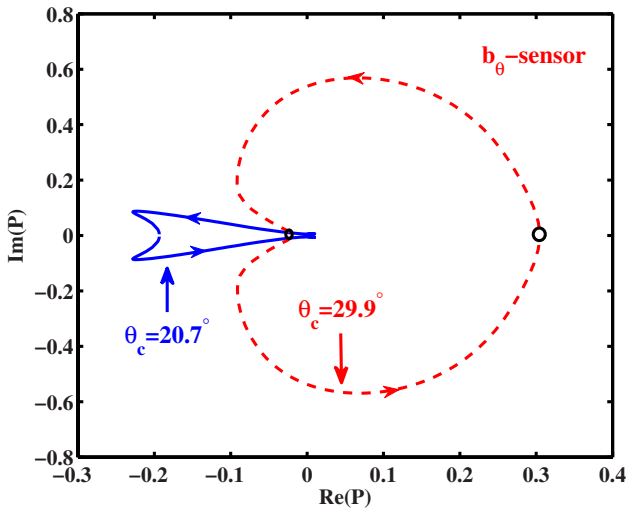

Figure 7. Nyquist plots of the MARS-F computed open loop transfer functions $P(j\omega)$ for the $n = 1$ RWM, for two poloidal locations of active coils, $\theta_c = 29.9°$ (dashed line) and $\theta_c = 20.7°$ (solid line), respectively. The other parameters are fixed at $d/a = 1.3, 1.35$, $r_f/a = 1.29$, $r_s/a = 1.29$, $\phi_U = 0°$, $\phi_L = 0°$, $\Omega_0 = 0$ and $\kappa_{||} = 1.5$. The arrows indicate the direction of increasing ω from $-\infty$ to $+\infty$. The circle indicates the location of $\omega = \infty$.

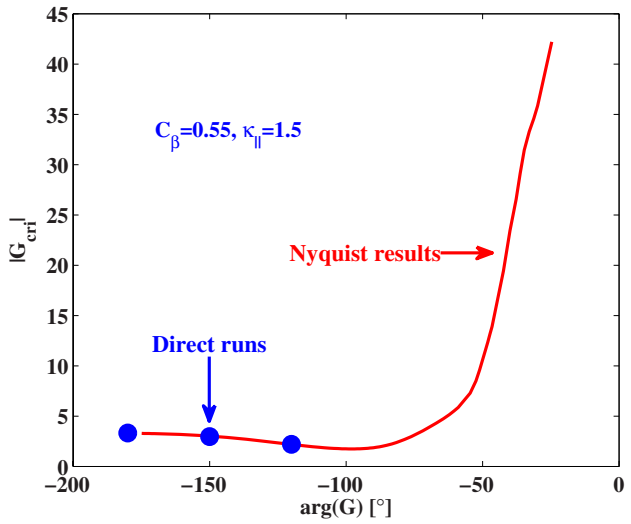

Figure 8. The computed critical proportional feedback gain amplitude for complete stabilization of the $n = 1$ RWM, versus the gain phase. Verified are two different approaches for computing the critical gain, either via the direct MARS-F feedback runs (dots) or via the transfer function based Nyquist analysis (solid line). The gain phases associated with the upper and lower rows of active coils are assumed the same $\phi_U = \phi_L = \arg(G)$. The other parameters are fixed at $d/a = 1.3, 1.35$, $r_f/a = 1.29$, $r_s/a = 1.29$, $C_\beta = 0.55$, $\theta_c = 29.9°$ and $\kappa_{||} = 1.5$.

that of figure 7). The other (dots) follows direct computation of the closed loop eigenvalue by MARS-F, solving together the MHD equations and the feedback equation for the active coil. The good agreement between these two approaches confirm the validity of feedback results reported here.

The results discussed above already point to the importance of choosing the feedback gain phase on the RWM stabilization, with two rows of active coils. For feedforward

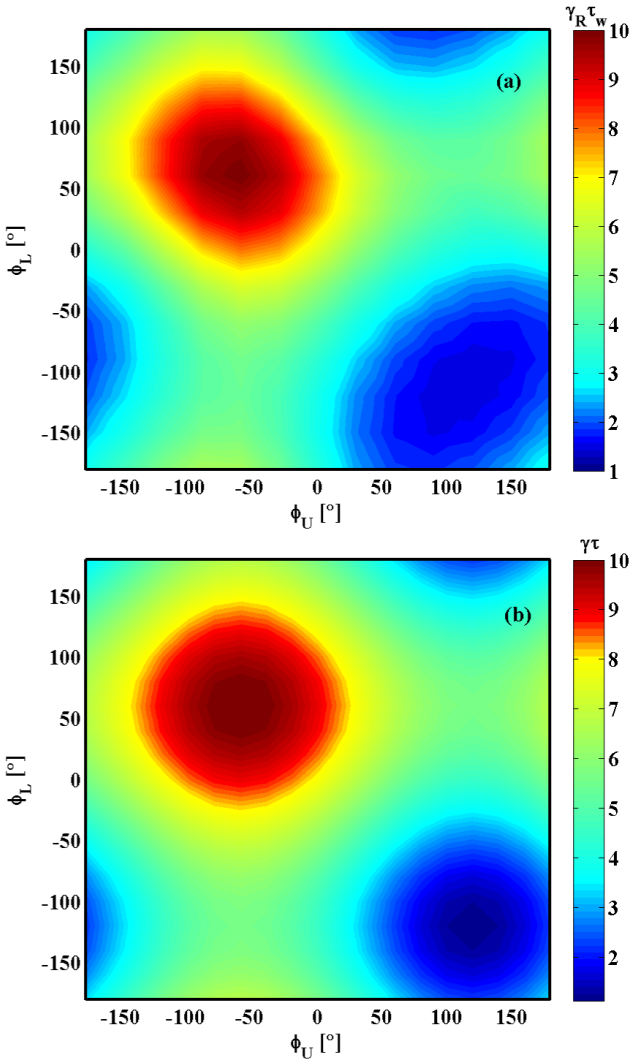

Figure 9. Contour plots of the $n = 1$ RWM growth rate in the 2D space for the proportional feedback gain phases $\phi_L - \phi_U$, calculated by (*a*) MARS-F and (*b*) a single-pole analytic model (see appendix). The parameters for MARS-F runs are fixed at $d/a = 1.3, 1.35$, $r_f/a = 1.29$, $r_s/a = 1.29$, $C_\beta = 0.55$, $\kappa_{||} = 1.5$, $\Omega_0 = 0$, $\theta_c = 29.9°$ and $|G| = 0.5$. The parameters in the analytic model are chosen as $\gamma_0 = 2.5 \times 10^{-4}$, $\omega_0 = 0$, $|R_U| = 2 \times 10^{-4}$, $\hat{\phi}_U = -120°$, $|R_L| = 2 \times 10^{-4}$, $\hat{\phi}_L = 120°$, $\tau_F = 2 \times 10^4$, $|G| = 0.5$ and $\alpha_D = 0$.

control of the type-I edge localized modes, this gain phase is translated into the so-called coil current phasing between the upper and lower rows of coils, which is shown to be again of critical importance [42]. Systematic studies of the effect of varying proportional feedback gain phase on the closed loop stability, in 2D parameter space of (ϕ_L, ϕ_U), are thus carried out in this work under various physics assumptions. Figure 9(*a*) shows the MARS-F computed results, assuming fluid model and vanishing plasma flow. Here we fix the gain amplitude at $|G| = 0.5$, being the same for two rows of active coils. We observe vast variation of the closed loop growth rate, as the feedback gain phase varies in the 2D parameter space. Global minimum (stabilization) and maximum (destabilization) are achieved at ($\phi_U = 120°$, $\phi_L = -120°$) and ($\phi_U = -60°$, $\phi_L = 60°$), respectively. The maximum and

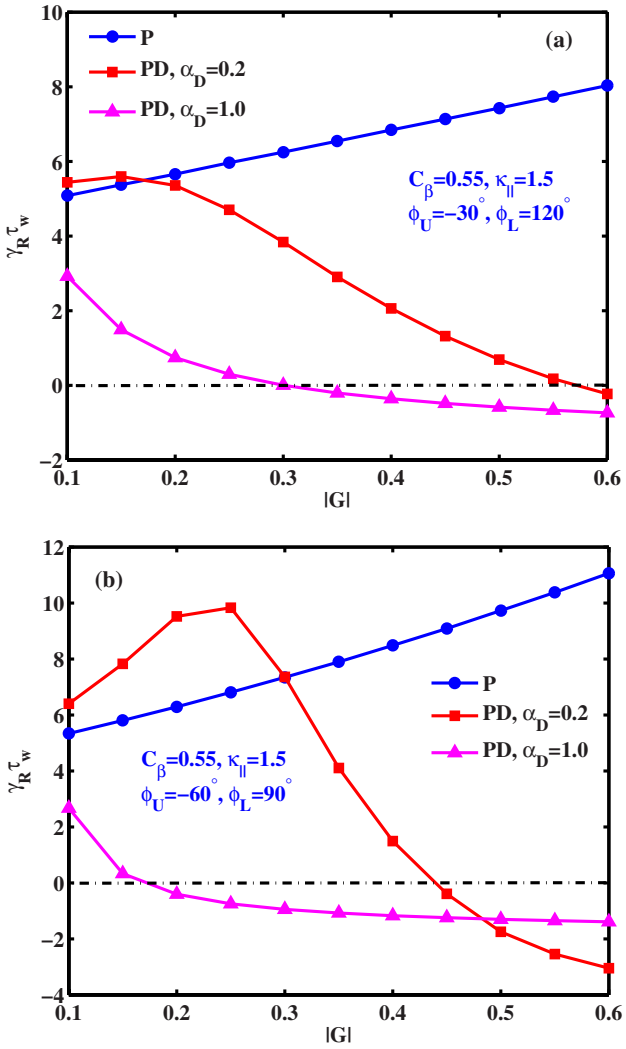

Figure 10. The MARS-F computed growth rate of the $n = 1$ RWM versus the amplitude of the feedback gain, assuming the gain phase associated with the upper and lower rows of coils to be (*a*) $\phi_U = -30°, \phi_L = 120°$ and (*b*) $\phi_U = -60°, \phi_L = 90°$. For each choice of the gain phase, compared are the proportional controller (circles), and the PD controllers with *D*/*P* gain ratio of $\alpha_D = 0.2$ (squares) and $\alpha_D = 1$ (triangles), respectively. The other parameters are fixed at $d/a = 1.3, 1.35$, $r_f/a = 1.29$, $r_s/a = 1.29$, $C_\beta = 0.55$, $\kappa_\| = 1.5$, $\Omega_0 = 0$ and $\theta_c = 29.9°$.

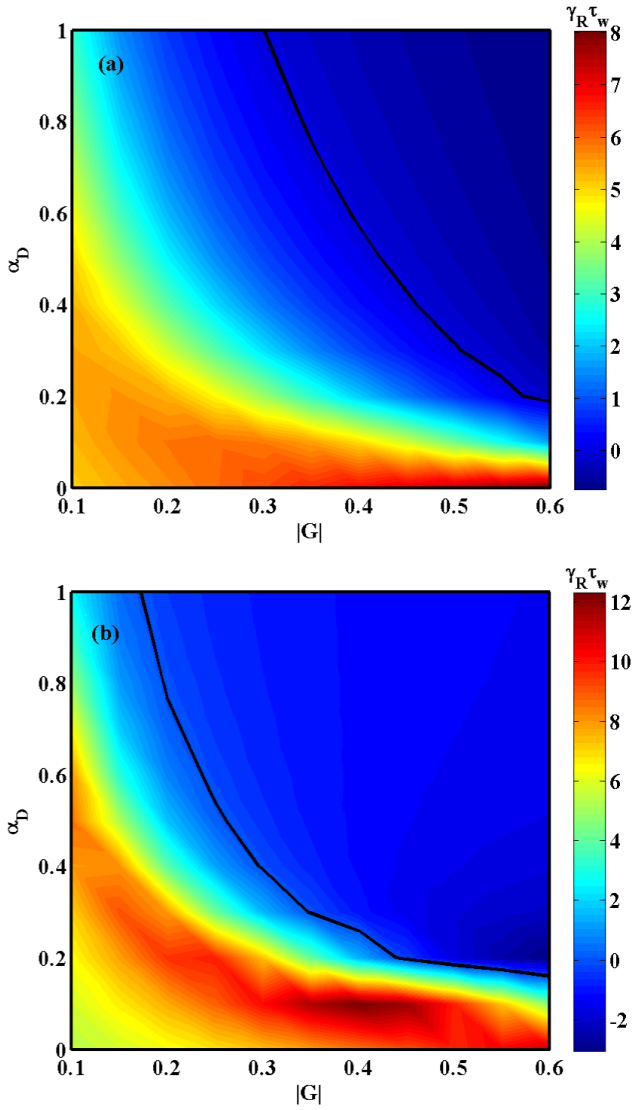

Figure 11. Contour plots of the MARS-F computed closed loop growth/damping rate of the $n = 1$ RWM in the 2D parameter space $\alpha_D - |G|$, assuming the gain phase associated with the upper and lower rows of coils to be (*a*) $\phi_U = -30°, \phi_L = 120°$ and (*b*) $\phi_U = -60°, \phi_L = 90°$. The other parameters are fixed at $d/a = 1.3, 1.35$, $r_f/a = 1.29$, $r_s/a = 1.29$, $C_\beta = 0.55$, $\kappa_\| = 1.5$, $\Omega_0 = 0$ and $\theta_c = 29.9°$. The solid curves indicate the stability boundaries in the 2D domain.

minimum solutions are well separated in the 2D space. The optima are reasonably robust against slight variations of the gain phasing. It is also evident that the gain phases that we have assumed in earlier studies (e.g. figures 5 and 6) fall in the region between the 'best' and the 'worst' control in figure 9.

It turns out that the MARS-F computed feedback gain phase scan results, shown in figure 9(*a*), can be qualitatively well re-produced by an analytic model (appendix) based on single pole approximation. With a proper choice of the parameters of the model, in particular the phase of the residuals (as complex numbers) associated with the open loop response to the upper and rows of coil currents, the MARS-F computed growth rate pattern (figure 9(*a*)) is well recovered by the analytic model (figure 9(*b*)). The phase of the residual of the open loop transfer function in essence reflects the toroidal phasing between the active coils and the poloidal sensors. Matching the MARS-F results and the analytic prediction, as shown in figure 9, indicates that this toroidal phasing is $\hat{\phi}_U = -120°$ and $\hat{\phi}_L = 120°$, respectively, for the upper and lower rows of coils in the HL-2M design. For the closed loop, the best gain phase is then the one that cancels the open loop residual phasing. This conclusion, valid for a proportional controller, is a theoretical insight offered by the simple analytic model.

Our study so far assumes a simple proportional feedback control scheme. A proper choice of PD controller further enhances the mode stabilization. This is particularly useful in the region of the 2D gain phase space shown in figure 9, where the closed loop destabilizes the RWM. Two examples are reported in figure 10. In each example, comparison

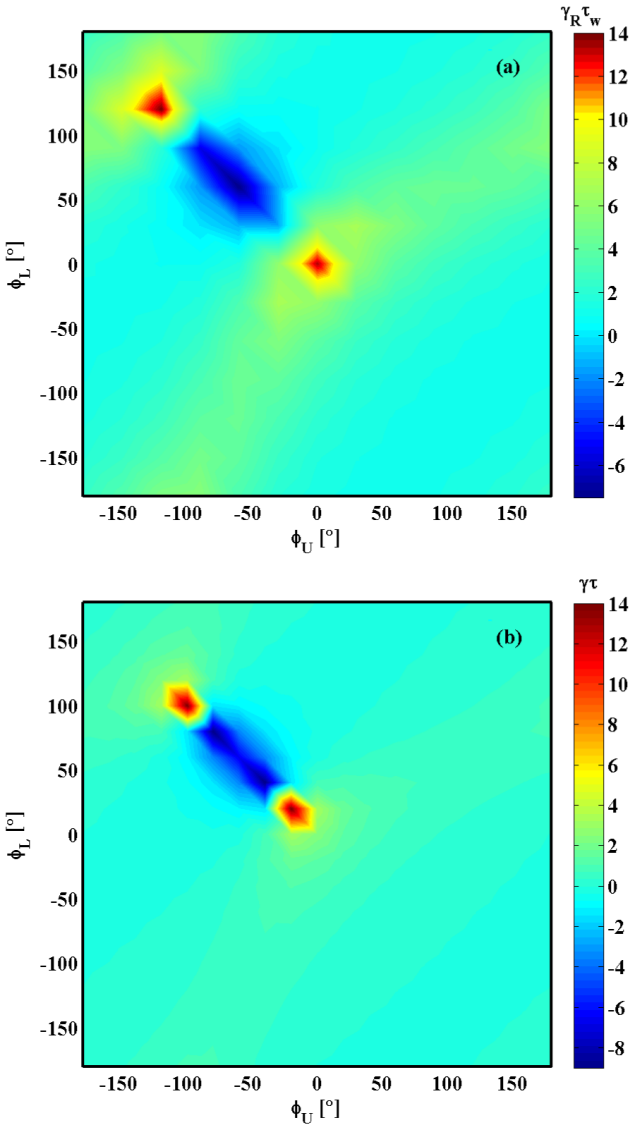

Figure 12. Contour plots of the closed loop growth/damping rate of the $n = 1$ RWM in the 2D feedback gain phase space $\phi_L - \phi_U$ with a PD controller ($\alpha_D = 0.2$), calculated by (*a*) MARS-F and (*b*) the analytic single-pole model (appendix). The other parameters in MARS-F runs are fixed at $d/a = 1.3, 1.35$, $r_f/a = 1.29$, $r_s/a = 1.29$, $C_\beta = 0.55$, $\kappa_\parallel = 1.5$, $\Omega_0 = 0$, $\theta_c = 29.9°$, and $|G| = 0.5$. The parameters in the analytical model are chosen as $\gamma_0 = 2.5 \times 10^{-4}$, $\omega_0 = 0$, $|R_U| = 3 \times 10^{-4}$, $\hat{\phi}_U = -120°$, $|R_L| = 3 \times 10^{-4}$, $\hat{\phi}_L = 120°$, $\tau_F = 2 \times 10^4$, $|G| = 0.5$.

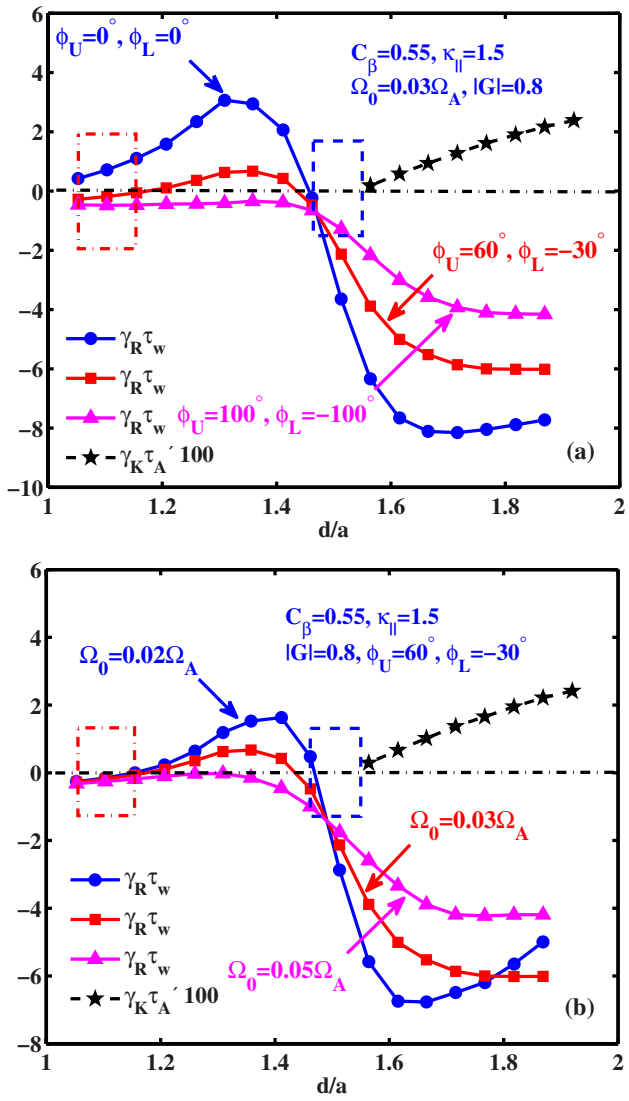

Figure 13. The MARS-F computed growth rate of the $n = 1$ RWM (solid lines) and the external kink mode (dashed lines) versus the wall minor radius, for (*a*) different choices of the proportional feedback gain phase $\phi_U = 0°, \phi_L = 0°$ (circles), $\phi_U = 60°, \phi_L = -30°$ (squares) and $\phi_U = 100°, \phi_L = -100°$ (triangles), respectively, at fixed plasma rotation frequency, and (*b*) different choices of the plasma rotation frequency $\Omega_0 = 0.02\Omega_A$ (circles), $\Omega_0 = 0.03\Omega_A$ (squares) and $\Omega_0 = 0.05\Omega_A$ (triangles), respectively, at fixed gain phase. The other parameters are fixed at $r_f/a = 1.29$, $r_s/a = 1.29$, $C_\beta = 0.55$, $\kappa_\parallel = 1.5$, $\theta_c = 29.9°$ and $|G| = 0.8$.

of the MARS-F computed closed loop growth rates is made between the P controller and the PD controller. A parameter α_D is introduced for the latter, labelling the ratio of the gain amplitude between the derivative and the proportional actions. Note the qualitative enhancement of the closed loop stability—from destabilization to stabilization—by adding the derivative action. A larger fraction of the derivative gain results in less critical gain amplitude, for full stabilization of the mode. This relation between the critical gain amplitude and the *D*/*P* gain ratio is further quantified in figure 11, for the same two choices of the gain phase as in figure 10. The solid curves represent the marginal stability of the closed loop.

As already demonstrated in figure 9(*a*), stabilization of the RWM is lost with the phase of the proportional gain being in the region of $0° < \phi_L < 90°$ and $-120° < \phi_U < -30°$. On the other hand, a PD controller can qualitatively modify the closed loop stability property in this area, as shown by figure 12. It is evident that addition of a moderate amount of *D*-action ($\alpha_D = 0.2$) in the control can fully suppress the RWM, in a gain phase domain which is otherwise destabilizing for the mode. On the other hand, this stabilization is not very robust, in the sense that a nearby region in the gain phase space exists, where the mode is strongly destabilized. All the aforementioned features of the PD stabilization are again

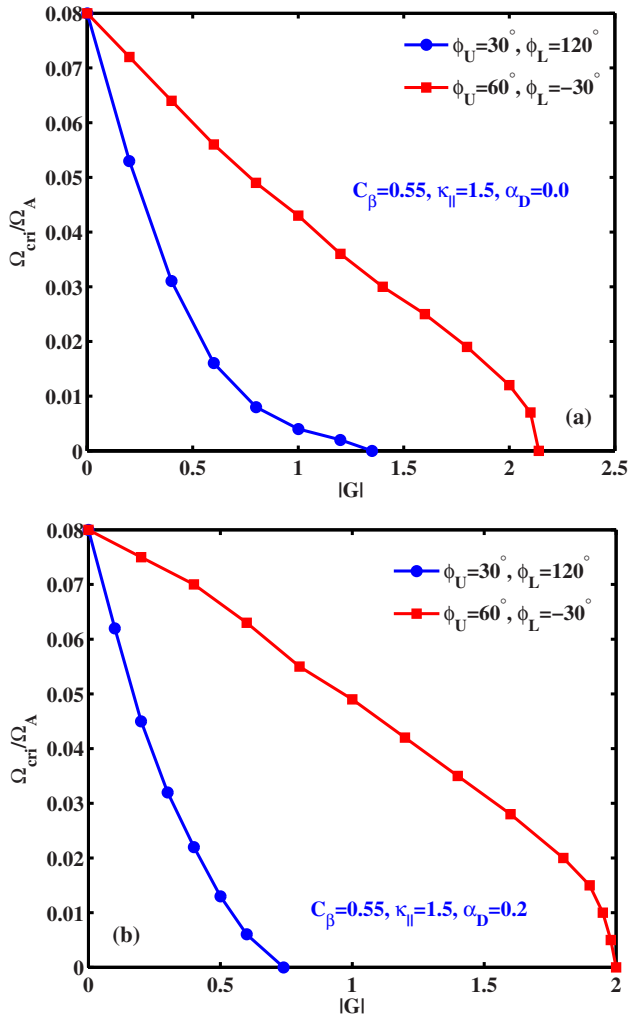

Figure 14. The MARS-F computed critical plasma rotation frequency for full stabilization of the $n = 1$ RWM versus the feedback gain amplitude, assuming (*a*) a proportional controller and (*b*) a PD controller with the *D*/*P* gain ratio α_D of 0.2. Compared are also results with two choices of the gain phase, $\phi_U = 30°, \phi_L = 120°$ (circles) and $\phi_U = 60°, \phi_L = -30°$ (squares), respectively. The other parameters are are fixed at $d/a = 1.3, 1.35$, $r_f/a = 1.29$, $r_s/a = 1.29$, $C_\beta = 0.55$, $\kappa_\parallel = 1.5$ and $\theta_c = 29.9°$.

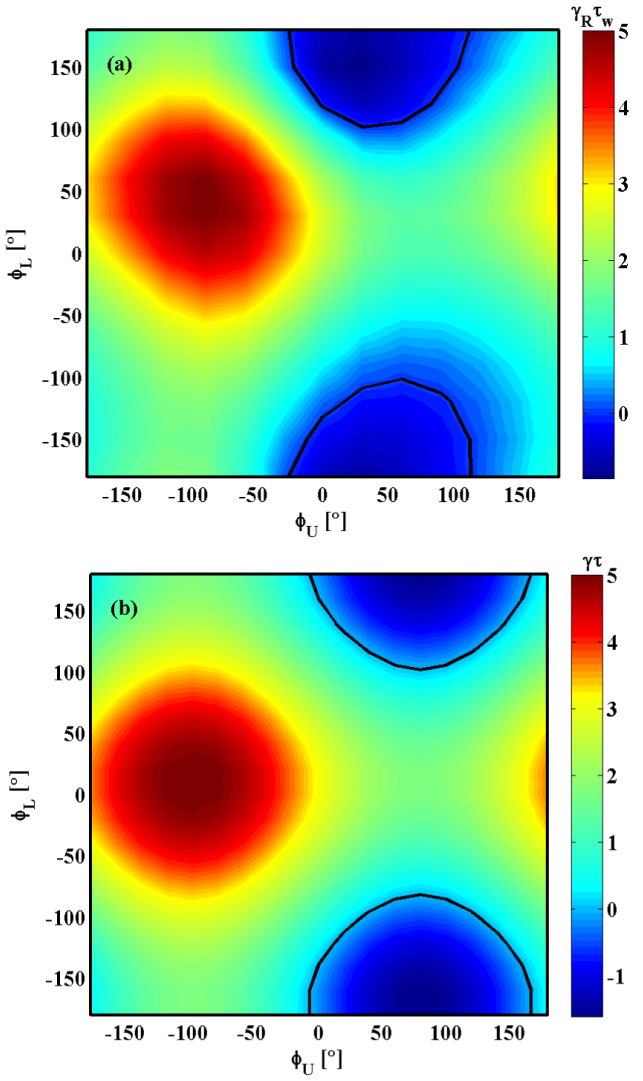

Figure 15. Contour plots for the closed loop growth/damping rate of the $n = 1$ RWM in the 2D gain phase space $\phi_L - \phi_U$, calculated by (*a*) MARS-F and (*b*) the analytic single-pole model. Assumed is a proportional control ($\alpha_D = 0$) in the presence of finite plasma flow in both cases. The other parameters for MARS-F runs are $d/a = 1.3, 1.35$, $C_\beta = 0.55$, $\kappa_\parallel = 1.5$, $\Omega_0 = 0.03\Omega_A$, $\theta_c = 29.9°$, and $|G| = 0.5$. The other parameters assumed in the analytic model are $\gamma_0 = 7.22 \times 10^{-5}$, $\omega_0 = 1.06 \times 10^{-4}$, $|R_U| = 1.4 \times 10^{-4}$, $\hat{\phi}_U = -80°$, $|R_L| = 1.4 \times 10^{-4}$, $\hat{\phi}_L = 170°$, $\tau_F = 2 \times 10^4$, $|G| = 0.5$. The solid curves indicate the stability boundaries in the 2D domain.

obtained by both MARS-F computations (figure 12(*a*)) and by the same single-pole analytic model described in appendix (figure 12(*b*)).

3.3. Synergetic effects of feedback, flow and kinetic damping on the RWM

In an earlier work [38], we investigated the synergetic effect between magnetic feedback and plasma flow on the RWM stabilization, based on the fluid model. We found that the combination of feedback and flow stabilization helps to open two stability windows in terms of the wall minor radius. As the first step in what follows, we figure out whether similar effect occurs for the HL-2M plasma.

Figure 13 shows that these two stable windows indeed appear as the resistive wall minor radius increases. One window opens when the wall is placed close to the plasma boundary. The other window opens when the resistive wall is located sufficiently far from the plasma boundary but still within the marginal stability point for the ideal wall stabilization. The second window is mainly associated with the flow stabilization of the RWM [5], whist the first window only occurs when magnetic feedback is in action. Moreover, the appearance of these two windows is relatively robust against variation of the gain phasing (figure 13(*a*)) or the plasma rotation frequency (figure 13(*b*)). At fixed rotation, the synergy is the strongest when the gain phasing is chosen to be close to the optimum (see figure 9)—in our case $\phi_U = 100°, \phi_L = -100°$ (figure 13(*a*)). The two stable windows merge into one large stable window in this case. In other words, the RWM is fully

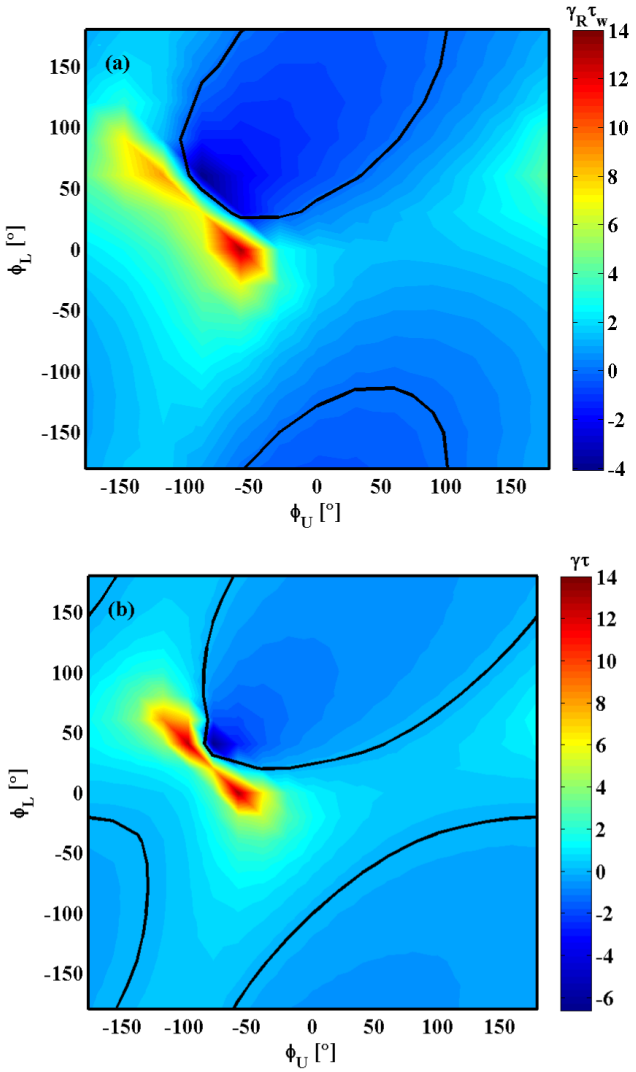

Figure 16. Contour plots for the closed loop growth/damping rate of the $n = 1$ RWM in the 2D gain phase space $\phi_L - \phi_U$, calculated by (*a*) MARS-F and (*b*) the analytic single-pole model. Assumed is a PD controller with the D/P gain ratio of $\alpha_D = 0.2$, in the presence of finite plasma flow in both cases. The other parameters for MARS-F runs are $d/a = 1.3, 1.35$, $C_\beta = 0.55$, $\kappa_\parallel = 1.5$, $\Omega_0 = 0.03\Omega_A$, $\theta_c = 29.9°$ and $|G| = 0.5$. The other parameters assumed in the analytic model are $\gamma_0 = 7.22 \times 10^{-5}$, $\omega_0 = 1.06 \times 10^{-4}$, $|R_U| = 2.5 \times 10^{-4}$, $\hat{\phi}_U = -100°$, $|R_L| = 2.5 \times 10^{-4}$, $\hat{\phi}_L = 150°$, $\tau_F = 2 \times 10^4$ and $|G| = 0.5$. The solid curves indicate the stability boundaries in the 2D domain.

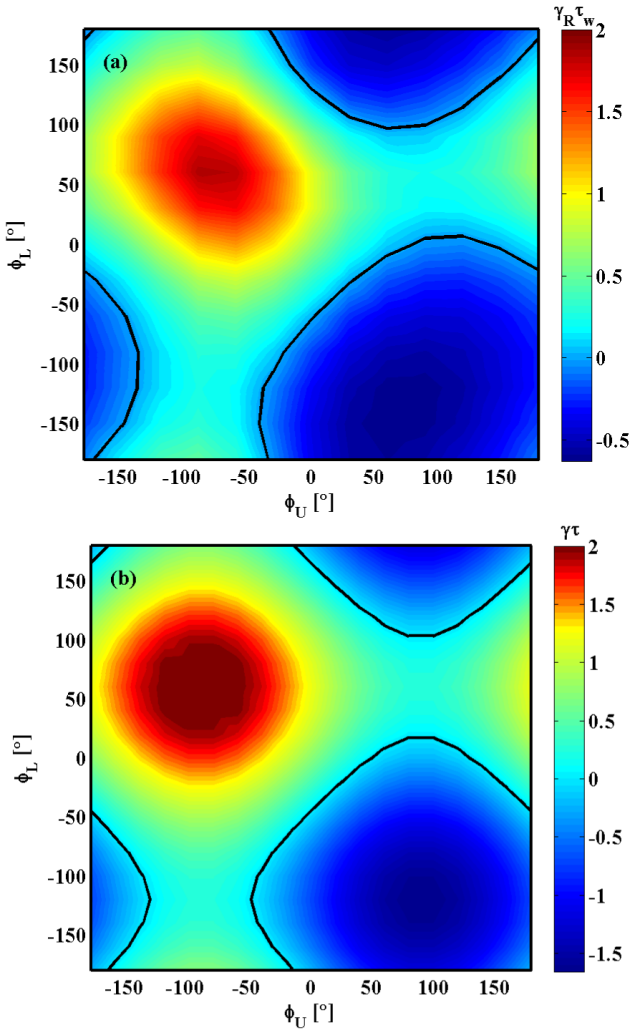

Figure 17. Contour plots for the closed loop growth/damping rate of the $n = 1$ RWM in the 2D gain phase space $\phi_L - \phi_U$, calculated by (*a*) MARS-K and (*b*) the analytic single-pole model. Assumed is a proportional control ($\alpha_D = 0$) in the presence of finite plasma flow in both cases. The MARS-K computations include precessional drift resonance of trapped thermal particles. The other parameters for MARS-K runs are $d/a = 1.3, 1.35$, $C_\beta = 0.55$, $\kappa_\parallel = 0.1$, $\Omega_0 = 0.01\Omega_A$, $\theta_c = 29.9°$, and $|G| = 0.5$. The other parameters assumed in the analytic model are $\gamma_0 = 1.04 \times 10^{-5}$, $\omega_0 = 1.93 \times 10^{-5}$, $|R_U| = 8 \times 10^{-5}$, $\hat{\phi}_U = -90°$, $|R_L| = 8 \times 10^{-5}$, $\hat{\phi}_L = 120°$, $\tau_F = 2 \times 10^4$, and $|G| = 0.5$. The solid curves indicate the stability boundaries in the 2D domain.

stabilized at any wall radius, up to the ideal-wall marginal point. Similar effect can be achieved with a less optimal choice of the gain phasing, but at the cost of increasing the flow speed (figure 13(*b*)).

The synergy effect is more clearly demonstrated in terms of the critical rotation frequency, that is required to (marginally) stabilize the RWM at a given feedback gain amplitude and phase. Figure 14 plots the critical rotation frequency versus the gain amplitude, for two choices of the gain phasing. The resistive wall position is now fixed according to the HL-2M design. The synergistic effect is evident. Moreover, the derivative control action further improves the synergy, by reducing the required critical rotation frequency at the same gain amplitude. For instance, with the gain phase of $\phi_U = 30°, \phi_L = 120°$, the required critical rotation frequency decreases about twice quicker with increasing gain amplitude, with inclusion of the derivative action.

Because of the synergistic effect, inclusion of the plasma flow also modifies the optimal choice of feedback gain phase for the RWM stabilization. This is illustrated by figure 15 (as compared to the case of vanishing flow presented in figure 9). Except the plasma rotation frequency, which is fixed at $\Omega_0 = 0.03\Omega_A$ in figure 15, all other parameters are identical to that of figure 9. Compared to figure 9, the optimal gain phase is shifted in the $\phi_L - \phi_U$ plane. Similar to figure 9, the

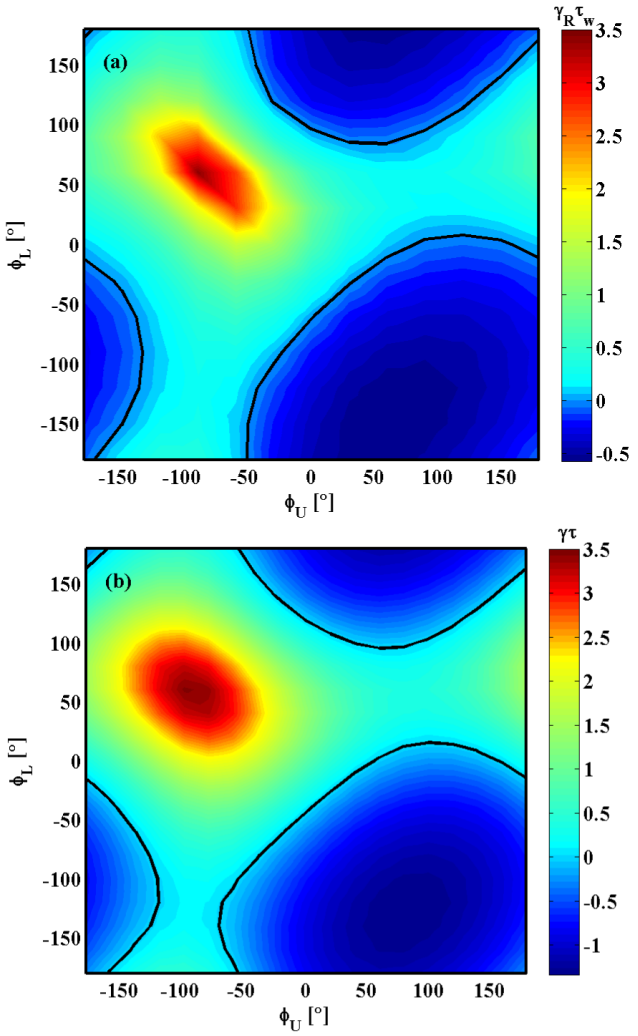

Figure 18. Contour plots for the closed loop growth/damping rate of the $n = 1$ RWM in the 2D gain phase space $\phi_L - \phi_U$, calculated by (*a*) MARS-K and (*b*) the analytic single-pole model. Assumed is a PD controller with the *D*/*P* gain ratio of $\alpha_D = 0.2$, in the presence of finite plasma flow in both cases. The MARS-K computations include precessional drift resonance of trapped thermal particles. The other parameters for MARS-K runs are $d/a = 1.3, 1.35$, $C_\beta = 0.55$, $\kappa_\parallel = 0.1$, $\Omega_0 = 0.01\Omega_A$, $\theta_c = 29.9°$, and $|G| = 0.5$. The other parameters assumed in the analytic model are $\gamma_0 = 1.04 \times 10^{-5}$, $\omega_0 = 1.93 \times 10^{-5}$, $|R_U| = 8 \times 10^{-5}$, $\hat{\phi}_U = -90°$, $|R_L| = 9 \times 10^{-5}$, $\hat{\phi}_L = 120°$, $\tau_F = 2 \times 10^4$, and $|G| = 0.5$. The solid curves indicate the stability boundaries in the 2D domain.

single-pole analytic model (figure 15(*a*)) can be used to match well the MARS-F computational results (figure 15(*b*)).

On top of the flow and proportional feedback stabilization as shown in figure 15, adding derivative control action ($\alpha_D = 0.2$ in figure 16) further enlarges the mode stabilization domain. The derivative action is particularly effective in the 'bad' gain phase region, where destabilization of the mode occurs. These observations are again confirmed by MARS-F (figure 16(*a*)) computations as well as by the analytic model (figure 16(*b*)).

Finally, we consider the synergy between magnetic feedback stabilization and drift kinetic damping of the RWM, in the presence of a finite plasma flow [39]. Figures 17 and 18 again show the 2D gain phase scan results, without and with the derivative action ($\alpha_D = 0.2$), respectively. We assume a relatively low plasma rotation frequency of $\Omega_0 = 0.01\Omega_A$, which leads to strong precessional drift resonance damping (see figure 3(*b*)). Compared to the fluid results (figure 15), drift kinetic damping substantially enlarges the stabilization domain in the feedback gain phase space. MARS-K results can again be reasonably well matched by the single-pole analytic model.

Comparison of figures 17 and 18 shows that the derivative action only slightly enhances the mode stabilization. This is because slower plasma flow ($\Omega_0 = 0.01\Omega_A$) does not drive fast mode rotation. The analytic model shows that the derivative action is indeed less effective when the open loop mode frequency is small (figure 18(*a*)).

4. Conclusions and discussion

In summary, we have carried out a systematic numerical investigation of the $n = 1$ RWM stabilization in HL-2M tokamak, using the MARS-F/K codes which include toroidal flow, magnetic feedback and drift kinetic physics. Simulations are performed for an advanced plasma scenario designed for HL-2M, with double-null configuration at 2 MA plasma current.

We identify the strong stabilizing role on the RWM due to the precession drift resonance effects associated with trapped thermal ions and electrons. For the design target plasma, corresponding to the pressure scaling factor of $C_\beta = 0.55$, the $n = 1$ RWM can be fully suppressed by the precessional drift kinetic resonance damping, at slow plasma rotation up to $\Omega_0 = 0.008\Omega_A$. Taking into account the potential pressure variation (C_β from 0 to 1), the mode stabilization is achieved at toroidal rotation frequency $\Omega_0 \leqslant 0.006\Omega_A$.

Feedback stabilization of the RWM, with two rows of magnetic coils as designed for HL-2M, is also achievable. However, the designed poloidal location ($\theta_c = 29.9°$) of the active coils is found not to be optimal for the RWM stabilization. The optimal coil location is $\theta_c = 20°$–$22°$. Several other factors can also significantly affect the control, including the choice of the feedback gain phase and the controller. Scan of the proportional feedback gain phase in 2D space, for the HL-2M coil design and with vanishing plasma flow, reveals a reasonably robust optimal value of ($\phi_U = 120°$, $\phi_L = -120°$). The opposite phasing, corresponding to the unfavorable choice for feedback, destabilizes the mode. With simple controllers (P versus PD) considered in this study, the derivative action significantly enhances the mode stabilization. The derivative action is particularly useful for reducing the unfavorable (destabilizing) domain in the 2D gain phase space.

MARS-F/K computations reveal the synergistic effects between the plasma flow damping (due to continuum wave resonances), drift kinetic damping, and magnetic feedback. The derivative control action brings another layer of enhancement for the mode stabilization. We emphasize that most

of the MARS-F/K 2D gain phase scan results can be qualitatively well re-produced by an analytic control model with single-pole approximation.

The findings from this work (i) confirm many of the previous results obtained for a generic toroidal plasma [38, 39]. Different from the previous work, the present study provides quantitative predictions for the stability of high-beta operational regimes specifically for the HL-2M device. The computed feedback results can serve as practical guidance for the RWM control coil design (e.g. the poloidal location of active coils) as well as the feedback configuration optimization (e.g. the feedback gain phasing) for HL-2M. Finally, the role of the derivative action is systematically analyzed in the present work, and is shown to be important for achieving synergistic stabilization of the RWM. This study was not carried out in our previous work [38, 39].

We have not considered the effect of energetic particles (EPs) on the RWM in HL-2M. The present design of HL-2M considers various heating systems: 15 MW of NBI, 8 MW of ECRH and 4 MW of LHCD. This leads to a 27 MW total heating capability. These heating sources (in particular NBI) will certainly create a significant amount of energetic ions. Transport modeling of the EPs distribution, density and pressure profiles are currently under way. Generally, the effect of EPs on the RWM can be two-fold: (i) EPs can provide additional stabilization to the RWM due to the interaction between the (large) banana orbit of trapped EPs and the mode (stabilization due to the so called third adiabatic invariant) [14, 43, 44]; (ii) on the other hand, there can be partial cancellation, between EPs and thermal particles, of the imaginary part of the drift kinetic energy (which also provides damping effect on the RWM) arising from the kinetic resonances between the mode and particles [45, 46]. Therefore, the eventual effect of EPs on the mode may be complicated. A dedicate modeling effort will be carried out in the future for HL-2M.

Acknowledgments

This work is supported by NSFC with Grant No. 11605046, 11575056, 11775071, 11505050, NMCFSP with Grant No. 2015GB105001 and the Royal Society K.C. Wong International Fellowship. The work is also supported by US DoE Office of Science under Contract Nos. DE-FG02-95ER54309 and DE-FC02-04ER54698. The project is also partly funded by the RCUK Energy Programme (grant number EP/P012450/1). To obtain further information on the data and models underlying this paper please contact PublicationsManager@ukaea.uk.

Appendix. A single-pole model of feedback gain Phase optimization for RWM control

Most of the MARS-F/K computational results with the feedback gain phase variation can be qualitatively explained by a simple analytic control model. Below we provide a detailed description of this model. We assume a single pole in the open loop transfer functions associated with the upper and lower rows of active coils

$$P_{\mathrm{U}}(s)=\frac{R_{\mathrm{U}}}{s-s_0},\quad P_{\mathrm{L}}(s)=\frac{R_{\mathrm{L}}}{s-s_0} \tag{A.1}$$

where $s_0=\gamma_0+\mathrm{i}\omega_0$ is the open loop RWM eigenvalue, $s=\gamma+\mathrm{i}\omega$ the closed loop eigenvalue. The residual factors, $R_{\mathrm{U}}=|R_{\mathrm{U}}|\,\mathrm{e}^{\mathrm{i}\hat{\phi}_{\mathrm{U}}}$ and $R_{\mathrm{L}}=|R_{\mathrm{L}}|\,\mathrm{e}^{\mathrm{i}\hat{\phi}_{\mathrm{L}}}$, are generally complex numbers, characterizing the mode response to the active coil currents. The phase of the residuals is largely related to the relative poloidal location between the active coils and the (outboard mid-plane poloidal) sensors. Within ideal MHD assumption and without plasma flow, s_0 is a real number. However, plasma flow and/or drift kinetic resonances can induce a finite frequency to the open loop eigenvalue.

Assuming a multiple-input-single-output control logic, the closed loop eigenvalue is determined by the solution of the characteristic equation

$$1+G_{\mathrm{U}}P_{\mathrm{U}}(s)+G_{\mathrm{L}}P_{\mathrm{L}}(s)=0, \tag{A.2}$$

where $G_{\mathrm{U}}=|G_{\mathrm{U}}|\,\mathrm{e}^{\mathrm{i}\phi_{\mathrm{U}}}(1+\alpha_{\mathrm{D}}s\tau_{\mathrm{F}})$ and $G_{\mathrm{L}}=|G_{\mathrm{L}}|\,\mathrm{e}^{\mathrm{i}\phi_{\mathrm{L}}}(1+\alpha_{\mathrm{D}}s\tau_{\mathrm{F}})$ are the (complex) feedback gains, generally including the proportional and derivative actions in this study. Here ϕ_{U} and ϕ_{L} represent the phase of the feedback gain, for the upper and lower rows of active coils, respectively. α_{D} measures the ratio of derivative to proportional gains, and τ_{F} is the L/R time of the active coils. If we further assume the same gain amplitude $|G_{\mathrm{U}}|=|G_{\mathrm{L}}|=|G|$, the closed loop eigenvalue can be easily calculated

$$\begin{cases}\gamma=\frac{(\gamma_0-C_1)(1+\alpha_{\mathrm{D}}\tau_{\mathrm{F}}C_1)+(\omega_0-C_2)\alpha_{\mathrm{D}}\tau_{\mathrm{F}}C_2}{(1+\alpha_{\mathrm{D}}\tau_{\mathrm{F}}C_1)^2+(\alpha_{\mathrm{D}}\tau_{\mathrm{F}}C_2)^2}\\ \omega=\frac{\omega_0-C_2-\gamma\alpha_{\mathrm{D}}\tau_{\mathrm{F}}C_2}{1+\alpha_{\mathrm{D}}\tau_{\mathrm{F}}C_1}\end{cases}, \tag{A.3}$$

$$\text{where}\quad\begin{cases}C_1=|G|\left[|R_{\mathrm{U}}|\cos\left(\hat{\phi}_{\mathrm{U}}+\phi_{\mathrm{U}}\right)+|R_{\mathrm{L}}|\cos\left(\hat{\phi}_{\mathrm{L}}+\phi_{\mathrm{L}}\right)\right]\\ C_2=|G|\left[|R_{\mathrm{U}}|\sin\left(\hat{\phi}_{\mathrm{U}}+\phi_{\mathrm{U}}\right)+|R_{\mathrm{L}}|\sin\left(\hat{\phi}_{\mathrm{L}}+\phi_{\mathrm{L}}\right)\right]\end{cases}.$$

Solution (A.3) indicates that, without derivative action, the optimal gain phase, that results in the strongest stabilization of the mode, corresponds to $\phi_{\mathrm{U}}=-\hat{\phi}_{\mathrm{U}}$, $\phi_{\mathrm{L}}=-\hat{\phi}_{\mathrm{L}}$, i.e. when the feedback gain phase exactly cancels that of the open loop residuals. In other words, the optimal gain phase does not depend on the open-loop mode eigenvalue. For a PD controller ($\alpha_{\mathrm{D}}>0.0$), however, the optimal gain phase will depend on the open loop eigenvalue.

ORCID iDs

C.J. Ham https://orcid.org/0000-0001-9190-8310

References

[1] Liu D.Q. *et al* 2013 *Fusion Eng. Des.* **88** 679–82
[2] Hender T.C. *et al* 2007 *Nucl. Fusion* **47** S128–202

[3] Chu M.S. and Okabayashi M. 2010 *Plasma Phys. Control. Fusion* **52** 123001
[4] Troyon F., Gruber R., Saurenmann H., Semenzato S. and Succi S. 1984 *Plasma Phys. Control. Fusion* **26** 209–15
[5] Bondeson A. and Ward D. 1994 *Phys. Rev. Lett.* **72** 2709
[6] Chu M.S., Greene J.M., Jensen T.H., Miller R.L., Bondeson A., Johnson R.W. and Mauel M.E. 1995 *Phys. Plasmas* **2** 2236
[7] Betti R. and Freidberg J.P. 1995 *Phys. Rev. Lett.* **74** 2949
[8] Gregoratto D., Bondeson A., Chu M.S. and Garofalo A.M. 2001 *Plasma Phys. Control. Fusion* **43** 1425–39
[9] Zheng L.J. and Kotschenreuther M. and Chu M. 2005 *Phys. Rev. Lett.* **95** 255003
[10] Hu B. and Betti R. 2004 *Phys. Rev. Lett.* **93** 105002
[11] Liu Y.Q. *et al* 2009 *Phys. Plasmas* **16** 056113
[12] Zheng L.J., Kotschenreuther M.T. and Van Dam J.W. 2009 *Nucl. Fusion* **49** 075021
[13] Liu Y.Q. *et al* 2010 *Plasma Phys. Control. Fusion* **52** 104002
[14] Berkery J.W., Sabbagh S.A., Reimerdes H., Betti R., Hu B., Bell R.E., Gerhardt S.P., Manickam J. and Podestá M. 2010 *Phys. Plasmas* **17** 082504
[15] Reimerdes H. *et al* 2007 *Phys. Rev. Lett.* **98** 055001
[16] Takechi M., Matsunaga G., Aiba N., Fujita T., Ozeki T., Koide Y., Sakamoto Y., Kurita G., Isayama A. and Kamada Y. 2007 *Phys. Rev. Lett.* **98** 055002
[17] Liu Y.Q., Bondeson A., Fransson C.M., Lennartson B. and Breitholtz C. 2000 *Phys. Plasmas* **7** 3681
[18] Okabayashi M. *et al* 2001 *Phys. Plasmas* **8** 2071
[19] Chu M.S. *et al* 2004 *Phys. Plasmas* **11** 2497
[20] Liu Y.Q., Bondeson A., Gribov Y. and Polevoi A. 2004 *Nucl. Fusion* **44** 232–42
[21] Strait E.J. *et al* 2004 *Phys. Plasmas* **11** 2505
[22] Fransson C.M., Lennartson B., Breitholtz C., Bondeson A. and Liu Y.Q. 2000 *Phys. Plasmas* **7** 4143
[23] Okabayashi M. *et al* 2005 *Nucl. Fusion* **45** 1715–31
[24] Sabbagh S., Bell R., Menard J., Gates D., Sontag A., Bialek J., LeBlanc B., Levinton F., Tritz K. and Yuh H. 2006 *Phys. Rev. Lett.* **97** 045004
[25] Drake J.R. *et al* 2005 *Nucl. Fusion* **45** 557–64
[26] Martin P. *et al* 2009 *Nucl. Fusion* **49** 104019
[27] Liu Y.Q., Chu M.S., Chapman I.T. and Hender T.C. 2008 *Phys. Plasmas* **15** 112503
[28] Liu Y.Q. and Bondeson A. 2000 *Phys. Rev. Lett.* **84** 907
[29] Wang Z.R., Guo S.C., Liu Y.Q. and Chu M.S. 2012 *Nucl. Fusion* **52** 063001
[30] Lütjens H., Bondeson A. and Sauter O. 1996 *Comput. Phys. Commun.* **97** 219
[31] Antonsen T.M. and Lee Y.C. 1982 *Phys. Fluids* **25** 132
[32] Porcelli F., Stankiewicz R., Kerner W. and Berk H.L. 1994 *Phys. Plasmas* **1** 470
[33] Liu Y.Q., Chapman I.T., Graves J.P., Hao G.Z., Wang Z.R., Menard J.E., Okabayashi M., Strait E.J. and Turnbull A. 2014 *Phys. Plasmas* **21** 056105
[34] Lao L., John H.S., Stambaugh R., Kellman A. and Pfeiffer W. 1985 *Nucl. Fusion* **25** 1611
[35] Bondeson A., Liu D.H., Söldner F.X., Persson M., Baranov Y.F. and Huysmans G.T.A. 1999 *Nucl. Fusion* **39** 1523
[36] Liu Y.Q. *et al* 2005 *Nucl. Fusion* **45** 1131–9
[37] Liu Y.Q., Chu M.S., Gimblett C.G. and Hastie R.J. 2008 *Phys. Plasmas* **15** 092505
[38] Xia G., Liu Y. and Liu Y.Q. 2014 *Plasma Phys. Control. Fusion* **56** 095009
[39] Xia G., Liu Y.Q., Liu Y., Hao G. and Li L. 2015 *Nucl. Fusion* **55** 093007
[40] Connor J.W., Hastie R.J. and Martin T.J. 1983 *Nucl. Fusion* **23** 1702
[41] Ward D.J. and Bondeson A. 1995 *Phys. Plasmas* **2** 1570
[42] Liu Y.Q. *et al* 2017 *Phys. Plasmas* **24** 056111
[43] Liu Y.Q. 2010 *Nucl. Fusion* **50** 095008
[44] Chapman I.T., Liu Y.Q., Asunta O., Graves J.P., Johnson T. and Jucker M. 2012 *Phys. Plasmas* **19** 052502
[45] Guo S.C., Liu Y.Q., Xu X.Y. and Wang Z.R. 2016 *Nucl. Fusion* **56** 076006
[46] Hao G.Z., Yang S.X., Liu Y.Q., Wang Z.X., Wang A.K. and He H.D. 2016 *Phys. Plasmas* **23** 062105